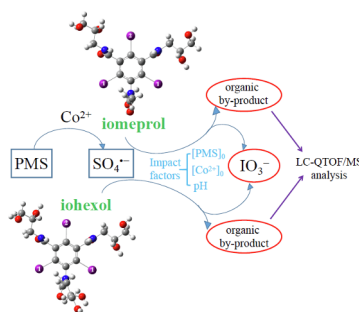# Oxidative degradation of iodinated X-ray contrast media (iomeprol and iohexol) with sulfate radical: An experimental and theoretical study

Xiaoxiao Wang[a], Zhaohui Wang[a,b,c,*], Yizhen Tang[d], Dongxue Xiao[e], Dong Zhang[e], Ying Huang[a], Yaoguang Guo[f], Jianshe Liu[a,g]

[a] State Environmental Protection Engineering Center for Pollution Treatment and Control in Textile Industry, College of Environmental Science and Engineering, Donghua University, Shanghai 201620, China
[b] Shanghai Key Laboratory of Urbanization and Ecological Restoration, School of Ecological and Environmental Sciences, East China Normal University, Shanghai 200241, China
[c] Institute of Eco-Chongming (IEC), Shanghai 200062, China
[d] School of Environmental and Municipal Engineering, Qingdao University of Technology, Fushun Road 11, 266033 Qingdao, China
[e] Chinese Academy of Fishery Sciences, East China Sea Fisheries Research Institute, Shanghai 200090, China
[f] School of Environmental and Materials Engineering, Shanghai Polytechnic University, Shanghai 201209, China
[g] Shanghai Institute of Pollution Control and Ecological Security, Shanghai 200092, China

## HIGHLIGHTS

- Iomeprol and iohexol can be effectively degraded by Co(II)-activated PMS.
- $IO_3^-$ is the major inorganic iodine released from iomeprol and iohexol.
- The possible transformation pathways of iomeprol and iohexol are proposed.
- Preferential deiodination order is theoretically predicted.

## GRAPHICAL ABSTRACT



## ARTICLE INFO

## ABSTRACT

It has already been known that oxidative degradation of organochlorine (e.g. chlorophenols) is accompanied by de novo formation of new polychlorinated compounds, however, whether the similar scenario can happen during decomposition of iodine-containing pollutants is completely unknown. Here degradation of two iodinated X-ray contrast media (ICM), iomeprol and iohexol, by sulfate radical generated through Co(II)-mediated activation of peroxymonosulfate (PMS) was investigated. The influencing parameters, such as the initial concentrations of PMS and Co(II), the initial solution pH and natural water constituents were examined. The pseudo-first-order rate constant of iomeprol in the PMS/Co(II) system is more than twice of iohexol, with values of $7.7 \times 10^{-2}$ and $3.5 \times 10^{-2}\,min^{-1}$, respectively, indicating that iomeprol seems more susceptible to radicals attack than iohexol. The bimolecular rate constants for reaction of sulfate radical ($SO_4^{\cdot-}$) with ICM were determined to be $1.8 \times 10^{10}\,M^{-1}\,s^{-1}$ and $7.9 \times 10^{9}\,M^{-1}\,s^{-1}$ for iomeprol and iohexol, respectively. The low degrees of mineralization and identification of iodinated intermediates of iomeprol and iohexol indicate that the degradation of iomeprol and iohexol in the Co/PMS system were incomplete. A de novo formation of new polyiodinated compounds would not happen because most of released inorganic iodine were ultimately oxidized to iodate ($IO_3^-$), rather than the reactive iodinated agents. Based on the identified byproducts and quantum

---

* Corresponding author.
  E-mail address: zhwang@des.ecnu.edu.cn (Z. Wang).

chemical calculation, eight main transformation pathways are proposed for the degradation of iomeprol and iohexol as follows: (a) deiodination; (b) hydrogen abstraction; (c) amide hydrolysis; (d) amino oxidation; (e) hydroxyl substituent; (f) transformed alkyl aromatic amides to aromatic carbamoyl; (g) dehydration; (h) oxidized primary alcohol groups to carboxyl groups.

## 1. Introduction

Iodinated X-ray contrast media (ICM), composed of 2,4,6-triiodinated benzoic acid derivatives, are applied in large quantities to enhance the visualization of organs or blood vessels during diagnostic tests. ICM cannot be removed effectively by conventional wastewater treatment plants because of their high polarity, persistence and biological inertness. In consequence, ICM at elevated concentrations ranging from $ng\,L^{-1}$ to $\mu g\,L^{-1}$ have been widely detected in surface water, groundwater and even raw drinking water supplies [1–4]. For instance, the concentration of iomeprol was reported as $0.38$–$6.10\,\mu g\,L^{-1}$ in the Besos river, Spain [3], $13\,\mu g\,L^{-1}$ in effluents of wastewater treatment plants in Germany [2]. ICM are the substantial contributors to the burden of adsorbable organic iodine (AOI) in the hospital wastewater [5]. In addition, ICM were recently identified as predominant organic iodine precursors for the formation of iodinated disinfection by-products (I-DBPs) during disinfection of drinking water [6,7]. The presence of I-DBPs in drinking waters has potential adverse health effects on human bodies since I-DBPs are generally more cytotoxic and genotoxic than their chlorinated and brominated analogs [8,9].

A number of technologies have been developed to remediate ICM contaminated wastewater and drinking water such as biodegradation and advanced oxidation processes (AOPs). The common hydroxyl radicals ($^{\bullet}OH$)-based AOPs for ICM treatment include ozonation [10], gamma irradiation [11,12], photooxidation [13,14], electrooxidation [15] and ultrasound [16]. Compared with $^{\bullet}OH$ ($E_0 = 2.59$–$2.74\,V$ in the acid solution; $E_0 = 1.77$–$1.91\,V$ in the neutral solution) [17,18], $SO_4^{\bullet-}$ has a higher standard redox potential ($E_0 = 2.5$–$3.1\,V$) [19] and a longer half-life with a wider pH range. Additionally, owing to its selectivity (electron transfer), $SO_4^{\bullet-}$ is more efficient to degrade organic compounds with the unsaturated bond and aromatic constituents than $^{\bullet}OH$ [17]. Thus, in recent years, $SO_4^{\bullet-}$-based AOPs have been suggested as an alternative in treating recalcitrant organic pollutants, such as azo-dyes, monochlorophenols and brominated compounds [20–23]. Since the available literature information is relatively rare on AOPs based on sulfate radicals ($SO_4^{\bullet-}$) for ICM degradation, the kinetics and mechanisms of ICM degradation by $SO_4^{\bullet-}$ are not explicit yet. Our previous study [19] indicated that in $SO_4^{\bullet-}$-induced degradation system, the released chlorine atoms from 2,4,6-trichlorophenol (TCP) could be involved in TCP degradation through de novo electrophilic addition reactions, generating several polychlorinated (chlorine atom number $\geq 3$) aromatics. Similarly, whether ICM can be degraded via deiodination process activated by sulfate radical and whether the released iodine atoms from ICM can participate in the re-iodination are worthy of investigations.

In the present work, cobalt-mediated activation of the peroxymonosulfate (PMS), a typical efficient method to generate $SO_4^{\bullet-}$ [24] was utilized. Two ICM, iomeprol and iohexol, were chosen as model

iodinated contaminants. The degradation kinetics as a function of the initial pH of the reaction solution, PMS and Co(II) concentrations, natural water constituents were evaluated. The fate of iodine and the degradation pathways of iomeprol and iohexol in the Co/PMS system were also investigated.

## 2. Experimental

### 2.1. Materials

Iomeprol ($> 98\%$) was purchased from Cato Research Chemicals Inc. (USA). PMS (Oxone®, $2KHSO_5 \cdot KHSO_4 \cdot K_2SO_4$, 95%) and iohexol were purchased from Sigma-Aldrich (Shanghai, China). Methanol (HPLC grade) was obtained from CNW Technologies GmbH (Germany). Formic acid (HPLC grade) and benzoic acid were supplied by Aladdin (Shanghai, China). $CoSO_4 \cdot 7H_2O$, $NaNO_2$, $NaOH$ and $H_2SO_4$ were of analytical grade and used without further purification. All sample solutions and stock solutions were prepared using Milli-Q water and stock solutions of all chemicals were prepared freshly.
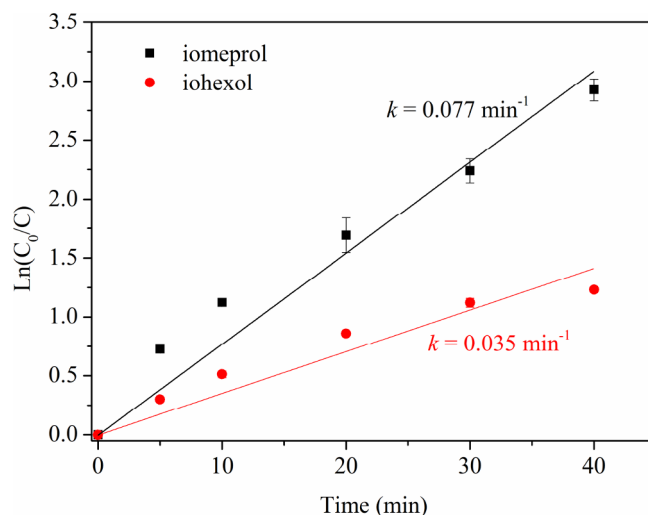


**Fig. 1.** Pseudo-first-order kinetic models of iomeprol (black line) and iohexol (red line) degradation. Experimental condition: for iomeprol, $[\text{iomeprol}]_0 = 0.02\,mM$, $[\text{PMS}]_0 = 0.16\,mM$, $[\text{Co}^{2+}]_0 = 0.008\,mM$, no pH adjustment; for iohexol, $[\text{iohexol}]_0 = 0.02\,mM$, $[\text{PMS}]_0 = 0.20\,mM$; $[\text{Co}^{2+}]_0 = 0.01\,mM$, no pH adjustment. (For interpretation of the references to colour in this figure legend, the reader is referred to the web version of this article.)
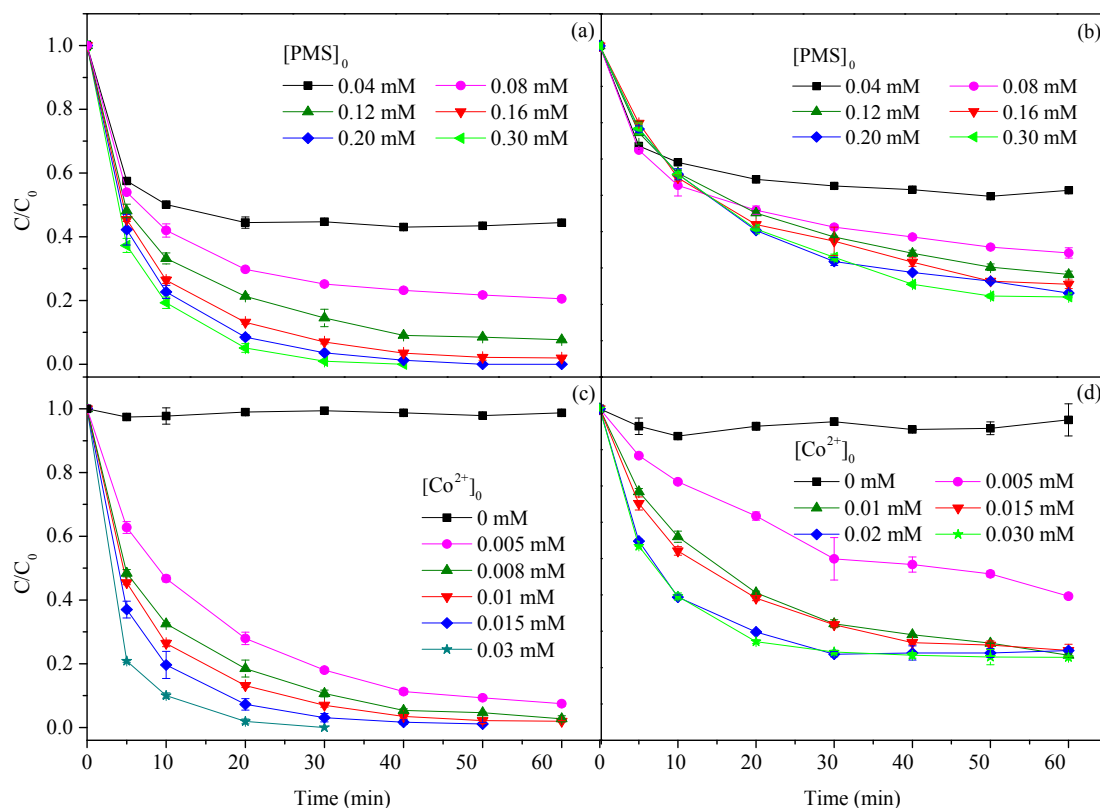
**Fig. 2.** Effects of initial concentrations of PMS and $Co^{2+}$ on the degradation of iomeprol (a, c) and iohexol (b, d). Experimental condition: $[ICM]_0 = 0.02$ mM, $[Co^{2+}]_0 = 0.01$ mM for (a, b); $[PMS]_0 = 0.16$ mM for (c); $[PMS]_0 = 0.20$ mM for (d), no pH adjustment.

## 2.2. Experimental procedures

All reactions were initiated by quickly mixing appropriate amounts of ICM, PMS and $CoSO_4$ solution in this order at room temperature ($25 \pm 2\,°C$), with the total volume of reaction solution of 50 mL, without the pH adjustment apart from the experiments concerning the influences of pH. Upon considering the effects of pH on degradation efficiency, pH of pre-mixed ICM/PMS solution and stock solution of $CoSO_4$ were adjusted by NaOH or $H_2SO_4$ solutions to the desired values, respectively, prior to their mixing. Continuous mixing was ensured by a magnetic stirrer during the reaction. Samples of 1 mL withdrawn at specific time intervals were immediately quenched with the same volume of methanol before the quantification of iomeprol and iohexol, while $NaNO_2$ as a quenching agent was added before the analysis of iodide ($I^-$), iodate ($IO_3^-$), mineralization and degradation products. The molar ratio of $NaNO_2$ to the residual oxidant was about 2:1. All experiments were performed in duplicates and the average data were displayed in the figures, with their standard deviations expressed as error bars. No significant pH change was observed after the reactions except the experiments examining the pH effect.

## 2.3. Analytical methods

Iomeprol, iohexol and benzoic acid were quantified by an Agilent 1260 HPLC system equipped with a CNW C18 column ($4.6 \times 250$ mm, $5.0\,\mu$m) at UV wavelength of 242, 245 and 230 nm, respectively. For iomeprol, the isocratic mobile phase was 10 mM phosphate buffer solution (pH 3.0): methanol (85:15, v:v) at a flow rate of $1$ mL min$^{-1}$. For iohexol, a mixture of ultrapure water with 0.1% formic acid and methanol was used as the mobile phase with the ratio of 80:20 (v:v) at a flow rate of $1$ mL min$^{-1}$. For benzoic acid, the mobile phase consisted of the mixture of 80% of 20 mM ammonium acetate and 20% of methanol at a flow rate of $1$ mL min$^{-1}$. The injection volume of the sample was $20\,\mu$L. The limits of quantification (LOQs) for iomeprol, iohexol and benzoic acid were 50.0, 25.0 and 100.0 $\mu$g L$^{-1}$, respectively. $I^-$ and $IO_3^-$ were detected by an ion chromatograph (Dionex-ICS2100) equipped with an Ionpac AS19 column (250 mm $\times$ 4.0 mm, 5.0 $\mu$m). The eluent was 35 mM KOH solution at a flow rate of 1.0 mL min$^{-1}$. The LOQs for $I^-$ and $IO_3^-$ were 5.0 and 3.0 $\mu$g L$^{-1}$, respectively. Total organic carbon (TOC) was determined using an Analytik Jena multi N/ C® 3100 TOC analyzer with a detection limit of 4.0 $\mu$g L$^{-1}$ to evaluate the degree of mineralization.
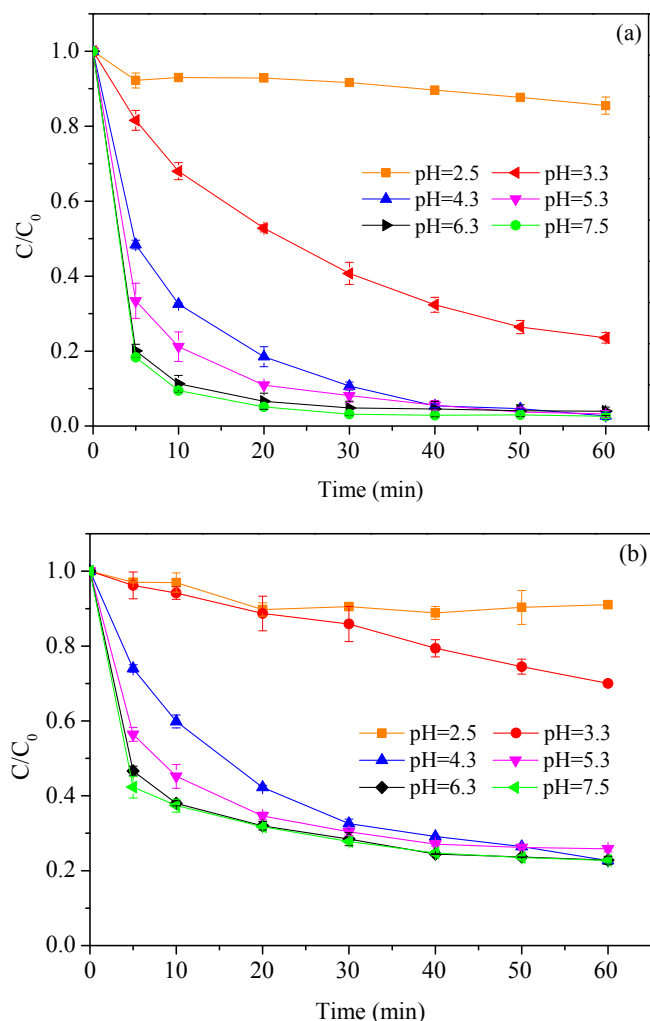
**Fig. 3.** Effects of initial solution pH on the degradation of iomeprol (a) and iohexol (b). Experimental condition: $[ICM]_0 = 0.02$ mM, $[PMS]_0 = 0.16$ mM, $[Co^{2+}]_0 = 0.008$ mM for (a); $[PMS]_0 = 0.20$ mM, $[Co^{2+}]_0 = 0.01$ mM for (b).

Ultra-performance liquid chromatography and quadrupole-time of flight mass spectrometer (UPLC-QTOF-MS, Agilent 1290UHPLC-6540QTOF, USA) were performed to identify and quantify the intermediate products formed during the degradation process. A sample volume of 20 μL was applied to an Agilent Zorbax Eclipse Plus-C18 column (2.1 × 50 mm, 1.8 μm). Column temperature was kept at 40 °C. For iomeprol, the mobile phase was A: acetonitrile and B: water with 0.03% acetic acid. The mobile phase flow was 0.2 mL/min and the following gradient was performed: 0–1 min, 10% A; 6–7 min, 90% A; 7.05–10 min, 10% A. For iohexol, acetonitrile (A) and water (B) were used as mobile phases. The mobile phase flow was 0.2 mL/min and the gradient elution was used: 0–1 min, 5% A; 3–8 min, 30% A; 9–10 min,

5% A. For QTOF–MS conditions, positive electrospray ionization (ESI +) over a mass scan range of 100–1100 $m/z$ was used for iomeprol. The mass spectrometer had a 10 L/min gas flow (N₂) at 325 °C, nebulizer pressure of 45 psig, and sheath gas flow of 12 L/min at 350 °C. The fragmentor voltage was set at 175 V while the skimmer voltage was set at 65 V. Negative electrospray ionization (ESI–) over a mass scan range of 100–1100 $m/z$ was used for iohexol. The mass spectrometer had a 8 L/min gas flow (N₂) at 300 °C, nebulizer pressure of 40 psig, and sheath gas flow of 6.5 L/min at 300 °C. The fragmentor voltage was set at 185 V while the skimmer voltage was set at 65 V. All possible formulas were obtained with Formula Calculator software according to the criteria that the mass error between the measured and the exact mass for a given chemical formula is less than 5 ppm. Molecular formulas were assigned to peaks with a signal-to noise ratio (S/N) greater than 4, in terms of stringent criteria with elemental combinations of $C_{5-80}H_{10-200}O_{0-40}N_{0-3}I_{0-3}$. The elemental ratios of H/C < 2.0 and O/C < 1.2 were used as further restrictions for formula calculation. The relevant parameters of the given formula are listed in Tables S1 and S2.

### 2.4. Theoretical investigations

Kinetic modeling was undertaken using a chemical modeling software, Kintecus 6.51 (http://www.kintecus.com). Table S3 summarizes all reactions used as inputs for the program. Most reaction rate constants are cited from the previous literature. The Kintecus program combined with a numerical routine was performed to estimate the unknown or poorly defined parameters by fitting degradation profiles.

All density functional theory (DFT) computations were performed using the Gaussian09 (Revision D.01) program [25]. Full geometry optimization of iomeprol and iohexol was carried out using the DFT method at the HF/3-21G level of theory. Then harmonic vibrational frequencies calculations were performed to ensure that the optimized geometries represent the local minima of potential energy surface and there are only positive eigen-values. The Natural Bond Orbital (NBO) charge population were calculated roughly employing quantum chemistry methods at the HF/3-21G levels of theory.

### 3. Results and discussion

#### 3.1. Degradation kinetics

As illustrated in Fig. 1, the degradation kinetics of iomeprol and iohexol as a function of time were fitted well with the pseudo-first-order kinetic model as shown in the following equation:

$$\ln(C_0/C) = kt \tag{1}$$

where $C_0$ is the initial ICM concentration, $C$ represents the residual concentration of ICM at time $t$ (min), $k$ is the degradation rate constant (min⁻¹), $t$ is the reaction time. Under certain conditions (0.16 mM PMS and 0.008 mM $Co^{2+}$ for 0.02 mM iomeprol; 0.2 mM PMS and 0.01 mM $Co^{2+}$ for 0.02 mM iohexol), the pseudo-first-order rate constant of iomeprol was found to be more than twice of iohexol, with values of 0.077 ($R^2 = 0.98$) and 0.035 ($R^2 = 0.92$) min⁻¹, respectively. As
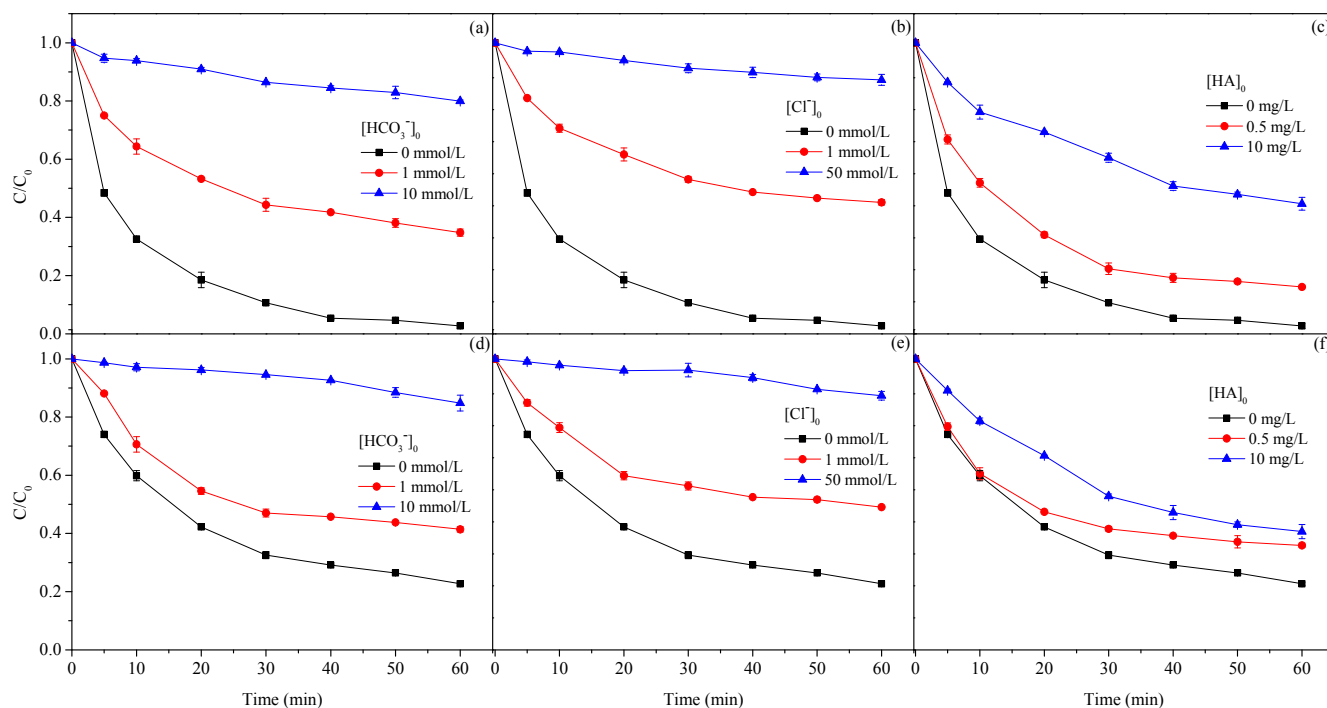
**Fig. 4.** Effects of alkalinity (a, d), $Cl^-$ (b, e), and NOM (c,f) on iomeprol (a,b,c) and iohexol (d,e,f) degradation in the PMS/Co(II) system. Experimental conditions: $[ICM]_0 = 0.02$ mM, $[PMS]_0 = 0.16$ mM, $[Co^{2+}]_0 = 0.008$ mM for (iomeprol); $[PMS]_0 = 0.20$ mM, $[Co^{2+}]_0 = 0.01$ mM for (iohexol), no pH adjustment.

expected, ICM degradation rate were inversely proportional to ICM concentration, as presented in Fig. S1. The first-order rate constant $k$ increased from $2.5 \times 10^{-2}$ min$^{-1}$ to $2.9 \times 10^{-1}$ min$^{-1}$ when iomeprol concentration decreased from 0.03 mM to 0.005 mM, while $k$ varied from $2.8 \times 10^{-2}$ min$^{-1}$ to $7.4 \times 10^{-2}$ min$^{-1}$ when iohexol concentration decreased from 0.03 mM to 0.005 mM. These results clearly demonstrate that iomeprol is more susceptible to radicals attack than iohexol.

The bimolecular rate constants of iomeprol and iohexol with $SO_4^{\bullet-}$ were determined by competition kinetics approach. Benzoic acid (BA) was selected as a reference compound with a known rate constant of $1.2 \times 10^9$ M$^{-1}$ s$^{-1}$ for the reaction with $SO_4^{\bullet-}$ [26]. The bimolecular rate constants for ICM and $SO_4^{\bullet-}$ reaction were measured based on Eq. (2), where $k_{SR,ICM}$ is the bimolecular rate constant for ICM and $SO_4^{\bullet-}$ reaction, and $k_{SR,BA}$ is the bimolecular rate constant for BA and $SO_4^{\bullet-}$ reaction.

$$\ln\left(\frac{[ICM]_t}{[ICM]_0}\right) = \frac{k_{SR,ICM}}{k_{SR,BA}}\ln\left(\frac{[BA]_t}{[BA]_0}\right) \tag{2}$$

The straight lines were obtained via plotting $\ln([ICM]_0/[ICM]_t)$ against $\ln([BA]_0/[BA]_t)$ (see Fig. S2 in supplementary information). Linear regression of these plots allowed for the determination of $k_{SR,ICM}$ which could be calculated from the slopes. The $k_{SR,ICM}$ values were found to be $1.8 \times 10^{10}$ M$^{-1}$ s$^{-1}$ and $7.9 \times 10^9$ M$^{-1}$ s$^{-1}$ for iomeprol and iohexol, respectively.

## 3.2. Impact factors

### 3.2.1. PMS concentration

The changes of ICM concentration ($C/C_0$) with reaction time at different initial PMS concentration are shown in Fig. 2, and the effects of initial concentrations of PMS on the first-order rate constant $k$ of iomeprol and iohexol are presented in Fig. S3. The degradation rates of both iomeprol and iohexol were significantly enhanced with the increase of PMS concentrations at a Co(II) concentration of 0.01 mM without pH adjustment (pH 4.3). When the initial PMS concentrations increased from 0.04 to 0.30 mM, the rate constant $k$ for the degradation of iomeprol in the first 30 min was elevated from $4.9 \times 10^{-2}$ to $1.5 \times 10^{-1}$ min$^{-1}$, with a removal rate increased from 55.6% to 99.0%. The improved degradation effectiveness should be attributed to the enhanced yield of $SO_4^{\bullet-}$ which is directly proportional to the oxidant concentrations under the same catalyst concentration. For iohexol, the rate constants of degradation ascended from $1.4 \times 10^{-2}$ to $3.5 \times 10^{-2}$ min$^{-1}$ as the initial PMS concentrations increased from 0.04 to 0.20 mM. Nevertheless, the degradation rate exhibited only a slight enhancement as the PMS concentration further increased to 0.3 mM, similar to the experimental results reported by Hu et al. [27]. This is mainly because that the excessive PMS, as a radical scavenger, could facilitate the transformation of $SO_4^{\bullet-}$ to $SO_5^{\bullet-}$, a less reactive radical (Eq. (3)).
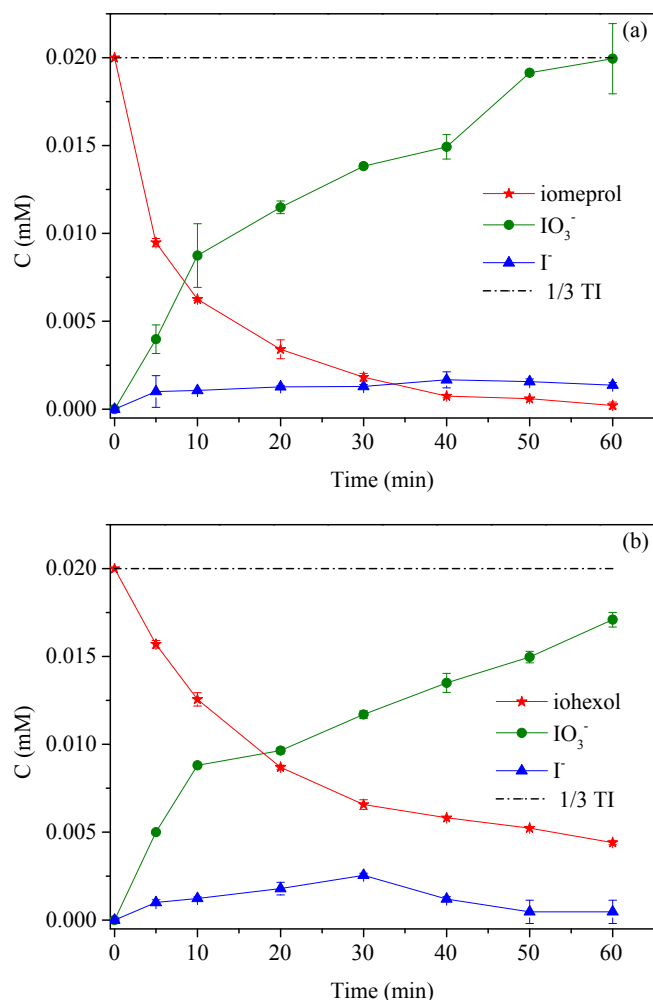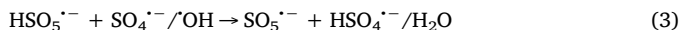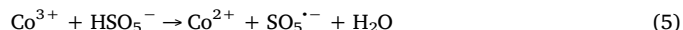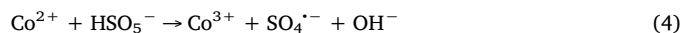
**Fig. 5.** The yields of $IO_3^-$ and $I^-$ during the degradation of iomeprol (a) and iohexol (b). Experimental condition: $[ICM]_0 = 0.02$ mM, $[PMS]_0 = 0.16$ mM, $[Co^{2+}]_0 = 0.008$ mM for (iomeprol); $[PMS]_0 = 0.20$ mM, $[Co^{2+}]_0 = 0.01$ mM for (iohexol), no pH adjustment.

$$HSO_5^{\bullet-} + SO_4^{\bullet-}/^{\bullet}OH \rightarrow SO_5^{\bullet-} + HSO_4^{\bullet-}/H_2O \qquad (3)$$

### 3.2.2. Co(II) concentration

The effect of catalyst concentration on the degradation of ICM was investigated by varying initial catalyst concentrations, as shown in Figs. 2 and S3. Nearly no iomeprol and iohexol degradation were observed in the absence of Co(II) due to the extremely slow self-generation of $SO_4^{\bullet-}$ from PMS. Upon increasing the $CoSO_4$ concentration, a faster and more efficient degradation of iomeprol occurred, especially evident in the first 10 min. This is ascribed to rapid decomposition of PMS motivated by the higher concentration of the catalyst. For iohexol, reaction rate and degradation efficiency were also increased in general, while no obvious enhancement was found when the initial $CoSO_4$ concentration

increased from 0.02 to 0.03 mM. The PMS oxidation catalyzed by transition metal ions was induced by redox reactions. Co(II) has the highest efficiency in initiating $SO_4^{\bullet-}$ generation from PMS (Eq. (4)), owing to the high reduction potential of $Co^{3+}/Co^{2+}$. The regeneration of $Co^{2+}$ with $HSO_5^-$, a crucial step to maintain the reactions with a low dosage of Co(II), is thermodynamically feasible (Eq. (5)) [28].

$$Co^{2+} + HSO_5^- \rightarrow Co^{3+} + SO_4^{\bullet-} + OH^- \qquad (4)$$

$$Co^{3+} + HSO_5^- \rightarrow Co^{2+} + SO_5^{\bullet-} + H_2O \qquad (5)$$

### 3.2.3. The initial pH values

Since $SO_4^{\bullet-}$ can be converted to $^{\bullet}OH$ in an alkaline solution [28], the influences of initial pH on the degradation of iomeprol and iohexol in the $SO_4^{\bullet-}$-based AOP system were merely evaluated at the pH range of 2.5–7.5. Fig. 3 shows that degradation of iomeprol and iohexol was most efficient at neutral pH (6.3–7.5). While the pH decreased from 6.3 to 4.3, the degradation rate of ICM was noticeably diminished but the extent of the overall degradation remained comparable at the end of 60 min. As pH decreased further to 3.3 and 2.5, the degradation efficiencies declined significantly, especially at pH 2.5. For example, for iomeprol, the initial reaction rate at the first 10 min was calculated to be $3.3 \times 10^{-4}$, $2.6 \times 10^{-4}$, and $5.0 \times 10^{-4}$ mmol/min, and the final degradation rate was 97.4%, 76.5%, and 14.5%, for initial pH values of 7.5, 3.3, and 2.5, respectively. It can be assumed that $HSO_5^-$ is the most dominant form of PMS present in solution at acidic and neutral pHs because that $pK_{a1}$ of $H_2SO_5$ is less than 0 and its $pK_{a2}$ is 9.4. Higher pH is beneficial to form $CoOH^+$ via the Co(II) hydrolysis (Eq. (6)), which is the dominant Co species responsible for PMS decomposition (Eq. (7)) [29].

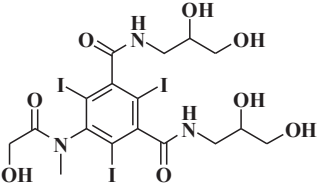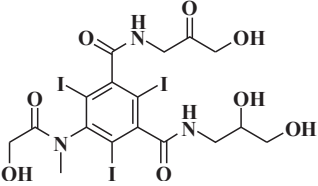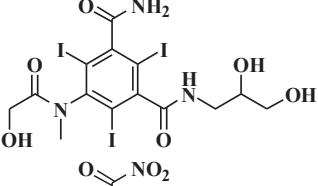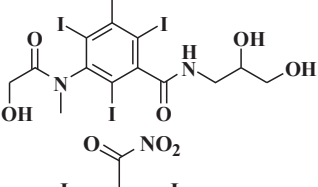$$Co^{2+} + H_2O \rightarrow CoOH^+ + H^+ \qquad (6)$$

$$CoOH^+ + HSO_5^- \rightarrow CoO^+ + H_2O + SO_4^{\bullet-} \qquad (7)$$
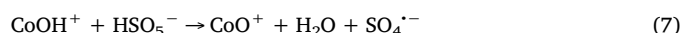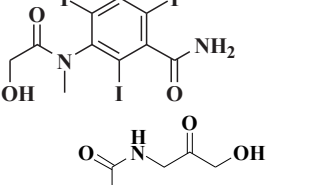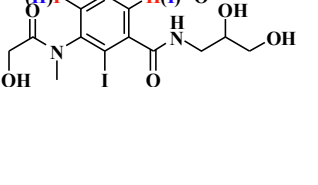
### 3.2.4. Natural water constituents

Owing to the ubiquity of various constituents in natural water environment, such as alkalinity, chloride ion and natural organic matter, the $SO_4^{\bullet-}$-based oxidative degradation may be affected. The effects of $HCO_3^-$, $Cl^-$ and humic acid (HA) on the ICM degradation were investigated. The experiments were carried out in the concentration of 1 and 10 mM for $HCO_3^-$, 1 and 50 mM for $Cl^-$, and in the concentration of 1 and 10 mg/L for HA, respectively. As shown in Fig. 4, different components exhibited some inhibitory effects on ICM degradation.

The degradation plots ($C/C_0$) of iomeprol and iohexol in the presence of 1 mM and 10 mM of $HCO_3^-$ are presented in Fig. 4a and d, respectively. $HCO_3^-$ inhibited the degradation of iomeprol and iohexol and the inhibitory effects became more pronounced as $HCO_3^-$ concentration inc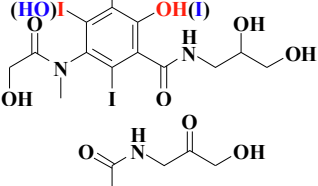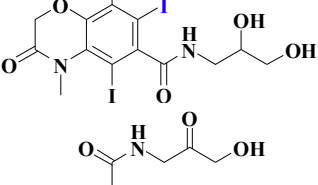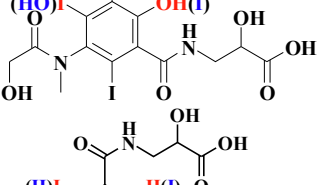reased. As the concentration of $HCO_3^-$ increased from 1 to 10 mM, the degradation constants of iomeprol dropped accordingly from 0.03 $min^{-1}$ to 0.004 $min^{-1}$, the corresponding degradation efficiency was 65.2% and 20.0% at 60 min. A similar decrease in rate constant and efficiency also occurred for iohexol degradation. The transformation of $SO_4^{\bullet-}$ to less reactive $CO_3^{\bullet-}$ ($k = 1.6 \times 10^6$ $M^{-1}s^{-1}$, Eq. (8)) is responsible for the diminishing degradation rates [30].

$$SO_4^{\bullet-} + HCO_3^- \rightarrow SO_4^{2-} + CO_3^{\bullet-} + H^+ \qquad (8)$$
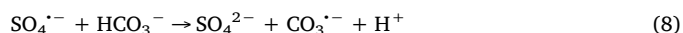
**Table 1**

The major transformation products of iomeprol identified from QTOF analysis.

| No. | Proposed structure | Formula | Mass (measured) | Exact mass |
|-----|--------------------|---------|-----------------|------------|
| 1 |  | $C_{17}H_{22}I_3N_3O_8$ | 776.854 | 776.8541 |
| 2 |  | $C_{17}H_{20}I_3N_3O_8$ | 774.838 | 774.8382 |
| 3 |  | $C_{14}H_{16}I_3N_3O_6$ | 702.817 | 702.8173 |
| 4 |  | $C_{14}H_{14}I_3N_3O_8$ | 732.791 | 732.7915 |
| 5 |  | $C_{11}H_8I_3N_3O_6$ | 658.754 | 658.7547 |
| 6 |  | $C_{17}H_{21}I_2N_3O_9$ | 664.936 | 664.9367 |
| 7 |  | $C_{17}H_{19}I_2N_3O_8$ | 646.926 | 646.9262 |
| 8 |  | $C_{17}H_{19}I_2N_3O_{10}$ | 678.915 | 678.9160 |
| 9 |  | $C_{17}H_{21}I_2N_3O_9$ | 664.936 | 664.9367 |

**Table 1** (*continued*)

| No. | Proposed structure | Formula | Mass (measured) | Exact mass |
|---|---|---|---|---|
| 10 | | $C_{17}H_{19}I_2N_3O_{10}$ | 678.915 | 678.9160 |
| 11 | | $C_{14}H_{15}I_2N_3O_8$ | 606.894 | 606.8949 |

As shown in Fig. 4b and e, in the presence of 1 mM and 50 mM $Cl^-$, the degradation efficiency of iomeprol was 54.8% and 13.5%, respectively. The scavenging of $SO_4^{•-}$ by $Cl^-$ and generation of much less reactive and more selective chlorine species such as HOCl, $Cl_2$ and $Cl_2^{•-}$ [20,31–33] should account for the adverse effect of $Cl^-$ on Co/PMS performance. A series of related chain reactions can be shown as follow (Eqs. (9)–(15)):

$$HSO_5^- + Cl^- \rightarrow SO_4^{2-} + HOCl \tag{9}$$

$$HSO_5^- + 2Cl^- + H^+ \rightarrow SO_4^{2-} + Cl_2 + H_2O \tag{10}$$

$$SO_4^{•-} + Cl \rightarrow SO_4^{2-} + Cl^• + H_2O \tag{11}$$

$$Cl^• + Cl^• \leftrightarrow Cl_2 \tag{12}$$

$$Cl^• + Cl^- \leftrightarrow Cl_2^{•-} \tag{13}$$

$$Cl_2^{•-} + Cl_2^{•-} \rightarrow Cl_2 + 2Cl^- \tag{14}$$

$$Cl_2 + H_2O \rightarrow HOCl + H^+ + Cl^- \tag{15}$$
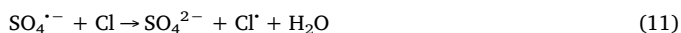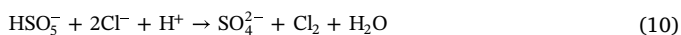
According to the explanation of Hu et al. [26], $Cl_2^{•-}$ is more inclined to selectively attack electron-rich groups. Iomeprol and iohexol, similar to iopamidol, have two amide groups with poor electron. Consequently, the attack of $Cl_2^{•-}$ on the two side chains may be inefficient.

Humic acid, as a common component of natural organic matter in natural water, its impact on the degradation rate should be considered. Fig. 4c and f show that the degradations of iomeprol and iohexol are suppressed in the presence of HA in aqueous solution, respectively. The observed iomeprol degradation rates in 60 min were 84.5% and 56.9% at 0.5 and 10 mg L$^{-1}$, respectively, and the corresponding $k$ values were 0.047 and 0.016 min$^{-1}$, respectively. The removal rates of iohexol were 64.1% and 59.3% at 0.5 and 10 mg L$^{-1}$ of HA, respectively. When the degradation kinetics of iohexol were fitted to a pseudo-first-order model, the values of $k$ were 0.028 and 0.017 min$^{-1}$ at 0.5 and 10 mg L$^{-1}$. Natural organic matter is electron-rich and can be easily attacked by the electrophilic radicals [34]. So ICM degradation was inhibited owing to the capture of $SO_4^{•-}$ by HA.

### 3.3. Fate of iodine

Fig. 5ab compare the release of iodine along with the oxidation of iomeprol and iohexol. $IO_3^-$ was found as a major inorganic iodine, with a final yield of 0.019 mM and 0.017 mM for iomeprol and iohexol, respectively. A recent study showed that in the CuO/PMS and $MnO_2$/PMS systems, $IO_3^-$ formation was considerable during the loss of total organic iodine in iopamidol, much higher than those of $I^-$ and free iodine [27]. Bichsel and von Gunten reported that $I^-$ could be transformed to $IO_3^-$ within seconds to minutes in aquacultures with the existence of oxidants, such as chlorine or ozone [35]. In the present system, the concentration of $IO_3^-$ was far higher than that of $I^-$, indicating that the majority of the iodine atom released from iomeprol and iohexol was oxidized to $IO_3^-$ by PMS or its derived radicals. Free iodine ($I_2$/HOI) was not quantified in the present work due to the interference of PMS oxidant during its measurement. However, Hu et al. [27] found that the formation of $I_2$/HOI was ignorable in comparison to $IO_3^-$. $IO_3^-$, nontoxic and comparatively stable, is the preferred sink of iodine in drinking waters. In the Co/PMS system, for both iomeprol and iohexol, the yields of $IO_3^-$ were less than a third of the total iodine content and the concentrations of $I^-$ were negligible. This implies that more than two-thirds of iodine atom from iomeprol or iohexol molecule still remained as organic iodines.

### 3.4. Kinetic modeling

Kintecus 6.51 is a smart program for chemical kinetics simulation, which can be easily operated within Microsoft Excel and has a built-in module for fitting/optimizing rate constants against experimental data. Taking iohexol for an example, Kintecus gives an acceptable fit to the experimental data for all the conditions tested (Figs. S4–S6). Fig. S7 also indicates that degradation of iohexol and formation of iodide can be well simulated in the present model, except for the $IO_3^-$ profile. The overestimated concentration of $IO_3^-$ from Kintecus at the beginning of iohexol destruction indicates that transformation of released iodine to $IO_3^-$ might undergo some intermediate steps, rather than a one-step process. The model also predicts minimal formation of iodide because it

**Table 2**
The major transformation products of iohexol identified from QTOF analysis.

| No. | Proposed structure | Formula | Mass (measured) | Exact mass |
|---|---|---|---|---|
| 1 |  | $C_{19}H_{26}I_3N_3O_9$ | 820.880 | 820.8803 |
| 2 |  | $C_{19}H_{24}I_3N_3O_9$ | 818.863 | 818.8647 |
| 3 |  | $C_{19}H_{25}I_2N_3O_{10}$ | 708.962 | 708.9629 |
| 4 |  | $C_{19}H_{27}I_2N_3O_{10}$ | 710.976 | 710.9786 |
| 5 |  | $C_{19}H_{27}I_2N_3O_{10}$ | 834.856 | 834.8596 |
| 6 |  | $C_{17}H_{20}I_3N_3O_{10}$ | 806.825 | 806.8283 |
| 7 |  | $C_{17}H_{18}I_3N_3O_8$ | 772.821 | 772.8228 |
| 8 |  | $C_{19}H_{23}I_2N_3O_9$ | 690.951 | 690.9524 |

**Table 2** (*continued*)

| No. | Proposed structure | Formula | Mass (measured) | Exact mass |
|---|---|---|---|---|
| 9 | | $C_{16}H_{18}I_3N_3O_7$ | 744.825 | 744.8279 |
| 10 | | $C_{14}H_{14}I_3N_3O_8$ | 732.790 | 732.7915 |
| 11 | | $C_{14}H_{12}I_3N_3O_8$ | 730.774 | 730.7759 |
| 12 | | $C_{14}H_{15}I_2N_3O_8$ | 606.893 | 606.8949 |
| 13 | | $C_{14}H_{15}I_2N_3O_9$ | 622.888 | 622.8898 |
| 14 | | $C_{14}H_{17}I_2N_3O_8$ | 608.908 | 608.9105 |
| 15 | | $C_{14}H_{17}I_2N_3O_9$ | 624.903 | 624.9054 |
| 16 | | $C_{14}H_{15}I_2N_3O_9$ | 622.888 | 622.8898 |

is easily oxidized by PMS or $SO_4^{\cdot-}/\cdot OH$.

### 3.5. Mineralization

The degrees of mineralization of iomeprol and iohexol in the Co/

PMS system were evaluated via analyzing the TOC removal efficiency. Very low TOC removal (< 7%) in both ICM systems is observed at 60 min (Fig. S8), when over 95% of iomeprol and 75% of iohexol has already been substantially degraded, respectively (Fig. 5). The mineralization rates of ICM improved with the reaction time. After 120 min,
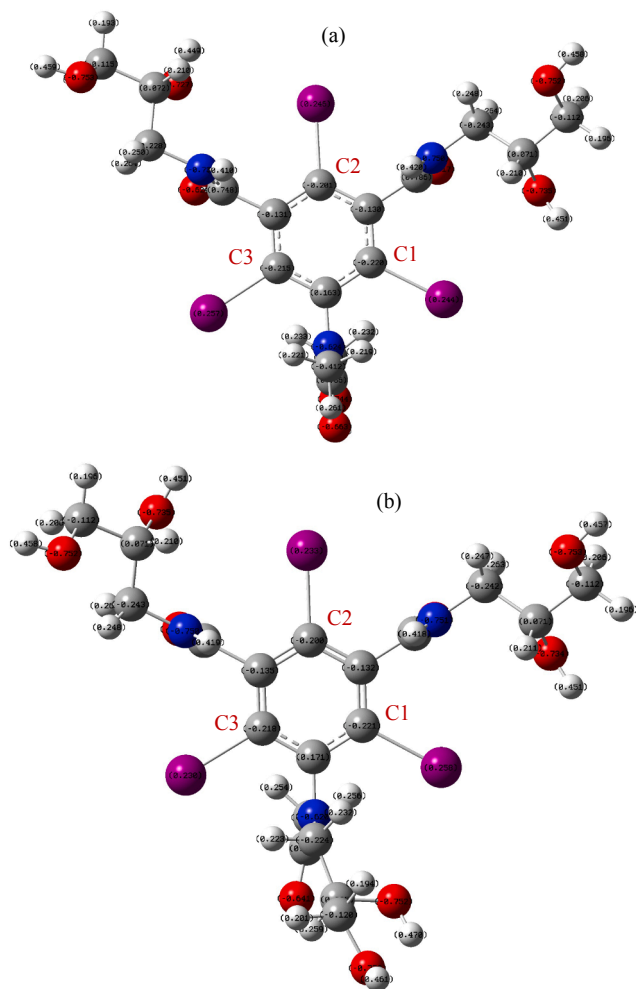
**Fig. 6.** Optimized geometric structure and mulliken atomic charges of iomeprol (a) and iohexol (b). Gray, blue, red, purple and white represent carbon, nitrogen, oxygen, iodine and hydrogen, respectively. (For interpretation of the references to colour in this figure legend, the reader is referred to the web version of this article.)

about 8.4% of iomeprol could be mineralized, and the TOC removal of iohexol was only about 6.5%. These low mineralization rates with high degradation rates of ICM imply that degradation of iomeprol or iohexol in the Co/PMS system probably only resulted from the side-chains cleavage of ICM molecule, such as C-I bond cleavage, rather than a complete destruction of the whole molecule.

### 3.6. Products identification and degradation pathways

By-products identification were conducted to elucidate the degradation mechanisms of iomeprol and iohexol in the Co/PMS system, respectively. For iomeprol, the identification of intermediates was based on the analysis of the total ion chromatograms (TIC) and the corresponding mass spectrum obtained by positive ion electrospray

high-resolution LC-MS. Mass spectrometric analysis was performed in negative ion mode for iohexol. Ten degradation intermediates (DIs) of iomeprol and fifteen DIs of iohexol were identified as listed in Tables 1 and 2.

To ascertain the deiodination order of three iodine atoms on the benzene ring, the Natural Bond Orbital (NBO) charge population were calculated roughly employing quantum chemistry methods at the HF/3-21G levels of theory. Atomic charge was used to describe the processes of electronegativity equalization and charge transfer in chemical reactions. The NBO charge population for all atoms is displayed in Fig. 6. All labeled carbon atoms exhibit positive charge in the two molecules, while three iodine atoms are negatively charged. It is worthy to mention that charge density on C1 and C3 carbon atoms varies slightly although they have the same proximal substituent groups. This may be resulted from the steric effects of substituent close to C1 and C3. The maximum negative atomic charge is observed for C1, indicating C1 site in the two compounds is more susceptible to electrophilic attack of sulfate and/or hydroxyl radicals. According to this prediction, degradation pathways of two ICM are proposed in Figs. 7 and 8.

As illustrated in Fig. 7, DI775 was generated from iomeprol by hydrogen abstraction reaction (1), which was further transformed to DI703 through de-alkylation process (2). Seitz et al. proposed three structures for DI775, with two types of aldehyde and ketone, and confirmed that the aldehyde and carbonyl functional groups occurred in the major products of iomeprol during ozonation [36], according to the derivatization method. The formation of aldehyde functional groups in the product with MW 775 was derived from the oxidation of aliphatic alcohols. The generation of carboxyl groups in some other products confirmed the existence and rationality of this type of the loss of 2 mass units. The de-alkylation process led to the conversion of alkyl (−CH$_2$(CO)CH$_2$OH) aromatic amides to aromatic carbamoyl. The de-alkylation reactions are in agreement with the recent studies of ICM degradation [37–39]. Similar cleavage of the N−C bond reactions was observed during biodegradation of iomeprol and iohexol [37]. Dong et al. and Wendel et al. reported that de-alkylation reactions should happen during degradation of iopamidol, a isomer of iomeprol, in iron activated persulfate systems and by chlorination [38,39]. The further amino oxidation (3) and subsequent de-alkylation in DI703 occurred, yielding DI733 and DI659, respectively. DI665 was generated from DI775 through the substitution of hydroxyl to iodine (4). This process includes two steps: (I) deiodination; (II) hydroxyl addition. SO$_4^{•−}$ attacking on a benzene ring via electron transfer, followed by elimination, leads to the formation of carbon-centered radicals which can react with H$_2$O quickly and form hydroxylated by hydrolysis [40,19]. The dehydration reaction (5) occurred in DI665, generating DI647, with a new ring formation. Additionally, DI665 was transformed to DI679 via the oxidation of a hydroxyl group, yielding a carboxyl group correspondingly (6). In another case, DI'665', considered as a isomer of DI665, was yielded from iomeprol via deiodination (7) and the oxidation of a primary alcohol group to a carboxyl group. It was further oxidized to generate DI'679' by an analogous oxidation of a primary alcohol group at the other side chain. Kormos et al. observed that oxidation of the primary alcohol groups occurred during biological transformation of iomeprol and iohexol [37]. A by-product containing a carboxyl group was generated from iohexol through oxidation of a primary alcohol group in UV/Fe$^{2+}$/H$_2$O$_2$ treatment [41]. The hydroxyl addition and the cleavage of '−CH$_2$CH(OH)CH$_2$OH' occurred in DI'665',
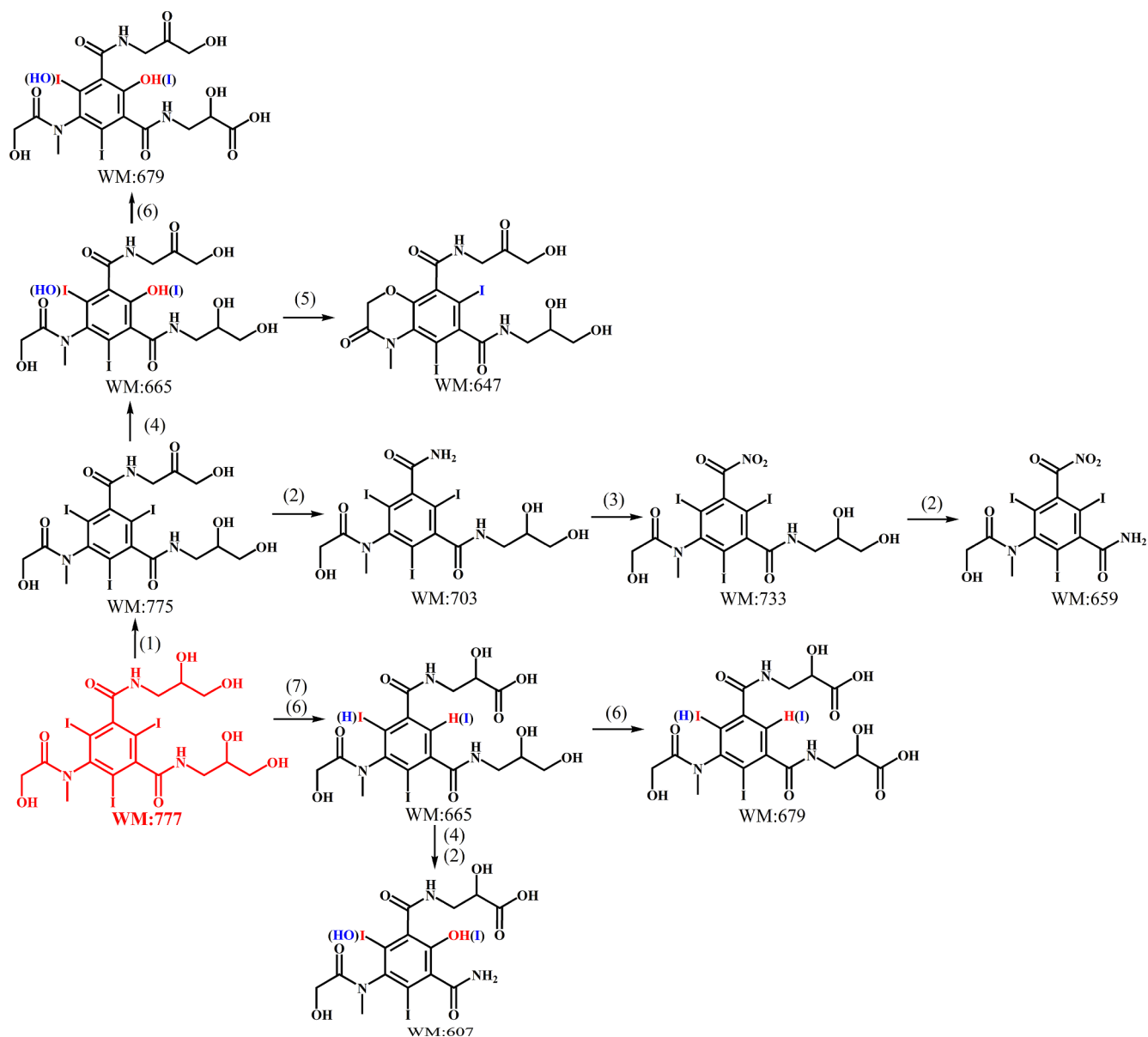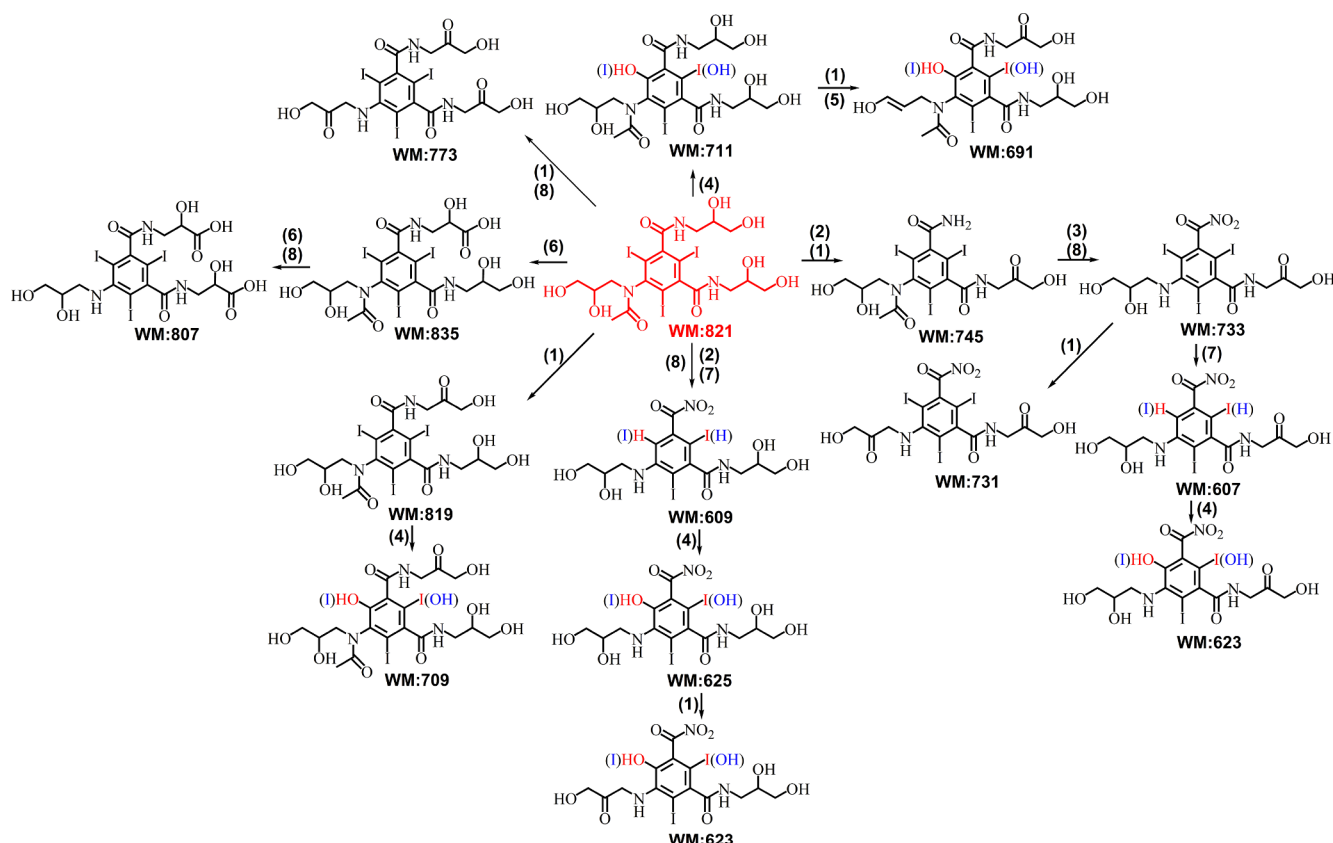
**Fig. 7.** Proposed iomeprol transformation pathways in the Co/PMS system. (1)–(7) denotes: (1) hydrogen abstraction; (2) transformed alkyl aromatic amides to aromatic carbamoyl; (3) amino oxidation; (4) hydroxyl substitution; (5) dehydration; (6) oxidized primary alcohol groups to carboxylates; (7) deiodination.

resulting in the formation of DI607. DI447 was transformed from io-meprol through substitution of three I atoms by OH group. The similar pathway for iohexol degradation is also proposed in Fig. 8 where an amide hydrolysis reaction (8) is observed.

## 4. Conclusion

This study investigated the kinetics and transformation pathways of iomeprol and iohexol in the Co(II)/PMS process. The degradation rate was significantly enhanced with the increase in PMS concentration, Co (II) concentration, and the initial solution pH. Natural water con-stituents (i.e., alkalinity, $Cl^-$ and natural organic matter) had inhibitory effects on ICM degradation to different degrees. The low TOC removal

efficiency and the identification of iodinated by-products elucidated that in the Co/PMS system iomeprol and iohexol could be degraded mostly via deiodination and the transformation of side chain rather than a complete degradation. The majority of the iodine released from iomeprol and iohexol was ultimately oxidized to $IO_3^-$. The iomeprol and iohexol degradation by Co/PMS mainly proceed through eight pathways: (a) deiodination; (b) hydrogen abstraction; (c) amide hy-drolysis; (d) amino oxidation; (e) hydroxyl substituent; (f) transformed alkyl aromatic amides to aromatic carbamoyl; (g) dehydration; (h) oxidized primary alcohol groups to carboxylates. The theoretical cal-culations further confirm the degradation kinetics and reaction path-ways.

**Fig. 8.** Proposed iohexol transformation pathways in the Co/PMS system. (1)–(8) denotes: (1) hydrogen abstraction; (2) transformed alkyl aromatic amides to aromatic carbamoyl; (3) amino oxidation; (4) hydroxyl substitution; (5) dehydration; (6) oxidized primary alcohol groups to carboxylates; (7) deiodination; (8) amide hydrolysis.

## Appendix A. Supplementary data

Supplementary data to this article can be found online at https://doi.org/10.1016/j.cej.2019.02.194.

## References

[1] C. Zhao, L.E. Arroyo-Mora, A.P. DeCaprio, V.K. Sharma, D.D. Dionysiou, K.E. O'Shea, Reductive and oxidative degradation of iopamidol, iodinated X-ray contrast media, by Fe(III)-oxalate under UV and visible light treatment, Water Res. 67 (2014) 144–153.

[2] J.L. Kormos, M. Schulz, T.A. Ternes, Occurrence of iodinated X-ray contrast media and their biotransformation products in the urban water cycle, Environ. Sci. Technol. 45 (2011) 8723–8732.

[3] B. Zonja, A. Delgado, S. Pérez, D. Barceló, LC-HRMS suspect screening for detection-based prioritization of iodinated contrast media photodegradates in surface waters, Environ. Sci. Technol. 49 (2015) 3464–3472.

[4] W. Ens, F. Senner, B. Gygax, G. Schlotterbeck, Development, validation, and application of a novel LC-MS/MS trace analysis method for the simultaneous quantification of seven iodinated X-ray contrast media and three artificial sweeteners in surface, ground, and drinking water, Anal. Bioanal. Chem. 406 (2014) 2789–2798.

[5] A. Putschew, S. Wischnack, M. Jekel, Occurrence of triiodinated X-ray contrast agents in the aquatic environment, Sci. Total Environ. 255 (2000) 129–134.

[6] Z. Wang, B. Xu, Y.L. Lin, C.Y. Hu, F.X. Tian, T.Y. Zhang, N.Y. Gao, A comparison of iodinated trihalomethane formation from iodide and iopamidol in the presence of organic precursors during monochloramination, Chem. Eng. J. 257 (2014) 292–298.

[7] T. Ye, B. Xu, Z. Wang, T.Y. Zhang, C.Y. Hu, L. Lin, S.J. Xia, N.Y. Gao, Comparison of iodinated trihalomethanes formation during aqueous chlor(am)ination of different iodinated X-ray contrast media compounds in the presence of natural organic matter, Water Res. 66 (2014) 390–398.

[8] S.D. Richardson, F. Fasano, J.J. Ellington, F.G. Grumley, K.M. Buettner, J.J. Evans, B.C. Blount, L.K. Silva, T.J. Waite, G.W. Luther, A.B. Mckague, R.J. Miltner, E.D. Wagner, M.J. Plewa, Occurrence and mammalian cell toxicity of iodinated disinfection byproducts in drinking water, Environ. Sci. Technol. 42 (2008) 8330–8338.

[9] M.T. Yang, X.R. Zhang, Comparative developmental toxicity of new aromatic halogenated DBPs in a chlorinated saline sewage effluent to the marine polychaete platynereis dumerilii, Environ. Sci. Technol. 47 (2013) 10868–10876.

[10] T.A. Ternes, J. Stüber, N. Herrmann, D. McDowell, A. Ried, M. Kampmann, B. Teiser, Ozonation: a tool for removal of pharmaceuticals, contrast media and musk fragrances from wastewater, Water Res. 37 (2003) 1976–1982.

[11] J. Jeong, J. Jung, W.J. Cooper, W. Song, Degradation mechanisms and kinetic studies for the treatment of X-ray contrast media compounds by advanced oxidation/reduction processes, Water Res. 44 (2010) 4391–4398.

[12] I. Velo-Gala, J.J. López-Peñalver, M. Sánchez-Polo, J. Rivera-Utrilla, Ionic X-ray contrast media degradation in aqueous solution induced by gamma radiation, Chem. Eng. J. 195–196 (2012) 369–376.

[13] F.X. Tian, B. Xu, Y.L. Lin, C.Y. Hu, T.Y. Zhang, N.Y. Gao, Photodegradation kinetics of iopamidol by UV irradiation and enhanced formation of iodinated disinfection by-products in sequential oxidation processes, Water Res. 58 (2014) 198–208.

[14] S. Pérez, P. Eichhorn, V. Ceballos, D. Barceló, Elucidation of phototransformation reactions of the X-ray contrast medium iopromide under simulated solar radiation using UPLC-ESI-QqTOF-MS, J. Mass. Spectrom. 44 (2009) 1308–1317.

[15] C.L. Eversloh, N. Henning, M. Schulz, T.A. Ternes, Electrochemical treatment of iopromide under conditions of reverse osmosis concentrates-Elucidation of the degradation pathway, Water Res. 48 (2014) 237–246.

[16] B. Ning, N.J.D. Graham, P.D. Lickiss, A comparison of ultrasound-based advanced oxidation processes for the removal of X-ray contrast media, Water Sci. Technol. 60 (2009) 2383–2390.

[17] P. Neta, R.E. Huie, A.B. Ross, Rate constants for reactions of inorganic radicals in aqueous solution, J. Phys. Chem. Ref. Data. 17 (1988) 1027–1284.

[18] G.V. Buxton, C.L. Greenstock, W.P. Helman, A.B. Ross, Critical review of rate constants for reactions of hydrated electrons, hydrogen-atoms and hydroxyl radicals (•OH/•O⁻) in aqueous solution, J. Phys. Chem. Ref. Data. 17 (1988) 513–886.

[19] L. Xu, R.X. Yuan, Y.G. Guo, D.X. Xiao, Y. Cao, Z.H. Wang, J.S. Liu, Sulfate radical-

induced degradation of 2,4,6-trichlorophenol: a de novo formation of chlorinated compounds, Chem. Eng. J. 217 (2013) 169–173.

[20] R.X. Yuan, S.N. Ramjuan, Z.H. Wang, J.S. Liu, Effects of chloride ion on degradation of acid orange 7 by sulfate radical-based advanced oxidation process: implications for formation of chlorinated aromatic compounds, J. Hazard. Mater. 196 (2011) 173–179.

[21] Y.G. Guo, J. Zhou, X.Y. Lou, R.L. Liu, D.X. Xiao, C.L. Fang, Z.H. Wang, J.S. Liu, Enhanced degradation of Tetrabromobisphenol A in water by a UV/base/persulfate system: kinetics and intermediates, Chem. Eng. J. 254 (2014) 538–544.

[22] C.L. Fang, X.Y. Lou, Y. Huang, M. Feng, Z.H. Wang, J.S. Liu, Monochlorophenols degradation by UV/persulfate is immune to the presence of chloride: illusion or reality, Chem. Eng. J. 323 (2017) 124–133.

[23] H.J. Peng, W. Zhang, L.Y. Xu, R.B. Fu, K.F. Lin, Oxidation and mechanism of dec-abromodiphenyl ether (BDE209) by thermally activated persulfate (TAP) in a soil system, Chem. Eng. J. 306 (2016) 226–232.

[24] G.P. Anipsitakis, D.D. Dionysiou, Radical generation by the interaction of transition metals with common oxidants, Environ. Sci. Technol. 38 (2004) 3705–3712.

[25] M.J. Frisch, G.W. Trucks, H.B. Schlegel, G.E. Scuseria, M.A. Robb, J.R. Cheeseman, G. Scalmani, V. Barone, B. Mennucci, G.A. Petersson, et al., Gaussian 09, Revision D.01, Gaussian, Inc., Wallingford, CT, 2009.

[26] P. Neta, V. Madhavan, H. Zemel, R.W. Fessenden, Rate constants and mechanism of reaction of $SO_4^{\cdot-}$ with aromatic compounds, J. Am. Chem. Soc. 99 (1997) 163–164.

[27] J. Hu, H.Y. Dong, J.H. Qu, Z.M. Qiang, Enhanced degradation of iopamidol by peroxymonosulfate catalyzed by two pipe corrosion products (CuO and $\delta$-MnO$_2$), Water Res. 112 (2017) 1–8.

[28] Y.H. Guan, J. Ma, X.C. Li, J.Y. Fang, L.W. Chen, Influence of pH on the formation of sulfate and hydroxyl radicals in the UV/peroxymonosulfate system, Environ. Sci. Technol. 45 (2011) 9308–9314.

[29] G.P. Anipsitakis, D.D. Dionysiou, Degradation of organic contaminants in water with sulfate radicals generated by the conjunction of peroxymonosulfate with Cobalt, Environ. Sci. Technol. 37 (2003) 4790–4797.

[30] C. Liang, Z.S. Wang, N. Mohanty, Influences of carbonate and chloride ions on persulfate oxidation of trichloroethylene at 20 degrees C, Sci. Total Environ. 370 (2006) 271–277.

[31] G.D. Fang, D.D. Dionysiou, Y. Wang, S.R. Abed, D.M. Zhou, Sulfate radical-based degradation of polychlorinated biphenyls: effects of chloride ion and reaction kinetics, J. Hazard. Mater. 227–228 (2012) 394–401.

[32] Y. Huang, B. Sheng, Z.H. Wang, Deciphering the degradation/chlorination mechanisms of maleic acid in the Fe(II)/peroxymonosulfate process: an often overlooked effect of chloride, Water Res. 145 (2018) 453–463.

[33] C.L. Fang, X.Y. Lou, Y. Huang, Monochlorophenols degradation by UV/persulfate is immune to the presence of chloride: illusion or reality? Chem. Eng. J. 323 (2017) 124–133.

[34] P.M. Gara, G.N. Bosio, M.C. Gonzalez, N. Russo, C.M.M. del, R.P. Diez, D.O. Mártire,, A combined theoretical and experimental study on the oxidation of fulvic acid by the sulfate radical anion, Photochem. Photobiol. Sci. 8 (2009) 992–997.

[35] Y. Bichsel, U.V. Gunten, Oxidation of iodide and hypoiodous acid in the disinfection of natural waters, Environ. Sci. Technol. 33 (1999) 4040–4045.

[36] W. Seitz, J.Q. Jiang, W. Schulz, W.H. Weber, D. Maier, M. Maier, Formation of oxidation by-products of the iodinated X-ray contrast medium iomeprol during ozonation, Chemosphere 70 (2008) 1238–1246.

[37] J.L. Kormos, M. Schulz, H.E. Kohler, T.A. Ternes, Biotransformation of selected iodinated X-ray contrast media and characterization of microbial transformation pathways, Environ. Sci. Technol. 44 (2010) 4998–5007.

[38] H.Y. Dong, Z.M. Qiang, J. Hu, C. Sans, Accelerated degradation of iopamidol in iron activated persulfate systems: roles of complexing agents and transformation of Iopamidol during chlorination, Chem. Eng. J. 316 (2017) 288–295.

[39] F.M. Wendel, C.L. Eversloh, E.J. Machek, S.E. Duirk, M.J. Plewa, S.D. Richardson, T.A. Ternes, Transformation of iopamidol during chlorination, Environ. Sci. Technol. 48 (2014) 12689–12697.

[40] Y.B. Ding, L.H. Zhu, N. Wang, H.Q. Tang, Sulfate radicals induced degradation of tetrabromobisphenol A with nanoscaled magnetic CuFe$_2$O$_4$ as a heterogeneous catalyst of peroxymonosulfate, Appl. Catal., B: Environ. 129 (2013) 153–162.

[41] S. Giannakis, M. Jovic, N. Gasilova, M.P. Gelabert, S. Schindelholz, J.M. Furbringer, H. Girault, C. Pulgarin, Iohexol degradation in wastewater and urine by UV-based advanced oxidation processes (AOPs): process modeling and by-products identification, J. Environ. Manage. 195 (2016) 1–12.